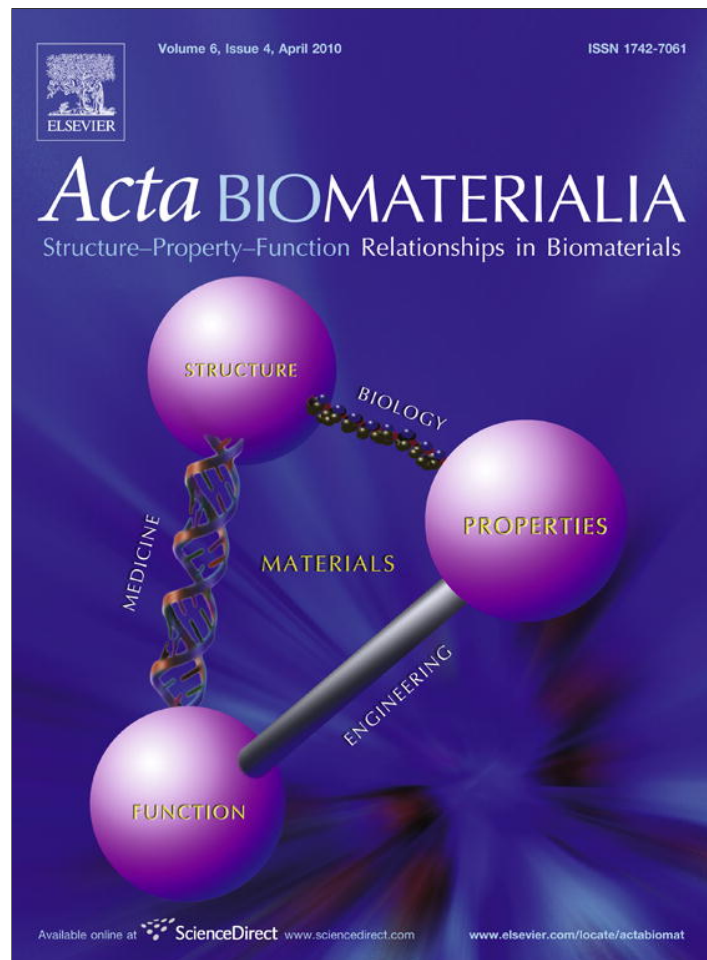


Provided for non-commercial research and education use.
Not for reproduction, distribution or commercial use.



This article appeared in a journal published by Elsevier. The attached copy is furnished to the author for internal non-commercial research and education use, including for instruction at the authors institution and sharing with colleagues.

Other uses, including reproduction and distribution, or selling or licensing copies, or posting to personal, institutional or third party websites are prohibited.

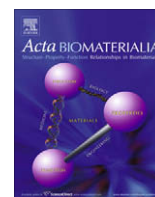
In most cases authors are permitted to post their version of the article (e.g. in Word or Tex form) to their personal website or institutional repository. Authors requiring further information regarding Elsevier's archiving and manuscript policies are encouraged to visit:

<http://www.elsevier.com/copyright>



Contents lists available at ScienceDirect

Acta Biomaterialia

journal homepage: www.elsevier.com/locate/actabiomat

Passive and active microrheology for cross-linked F-actin networks *in vitro*

Hyungsuk Lee^a, Jorge M. Ferrer^b, Fumihiko Nakamura^c, Matthew J. Lang^{a,b}, Roger D. Kamm^{a,b,*}

^a Department of Mechanical Engineering, Massachusetts Institute of Technology, Cambridge, MA 02139, USA

^b Department of Biological Engineering, Massachusetts Institute of Technology, Cambridge, MA 02139, USA

^c Translational Medicine Division, Brigham and Women's Hospital, Department of Medicine, Harvard Medical School, Boston, MA 02115, USA

ARTICLE INFO

Article history:

Received 26 May 2009

Received in revised form 16 September 2009

Accepted 27 October 2009

Available online 31 October 2009

Keywords:

F-actin network

Shear modulus

α -Actinin

Filamin

Gelsolin

ABSTRACT

Actin filament (F-actin) is one of the dominant structural constituents in the cytoskeleton. Orchestrated by various actin-binding proteins (ABPs), F-actin is assembled into higher-order structures such as bundles and networks that provide mechanical support for the cell and play important roles in numerous cellular processes. Although mechanical properties of F-actin networks have been extensively studied, the underlying mechanisms for network elasticity are not fully understood, in part because different measurements probe different length and force scales. Here, we developed both passive and active microrheology techniques using optical tweezers to estimate the mechanical properties of F-actin networks at a length scale comparable to cells. For the passive approach we tracked the motion of a thermally fluctuating colloidal sphere to estimate the frequency-dependent complex shear modulus of the network. In the active approach, we used an optical trap to oscillate an embedded microsphere and monitored the response in order to obtain network viscoelasticity over a physiologically relevant force range. While both active and passive measurements exhibit similar results at low strain, the F-actin network subject to high strain exhibits non-linear behavior which is analogous to the strain-hardening observed in macroscale measurements. Using confocal and total internal reflection fluorescent microscopy, we also characterize the microstructure of reconstituted F-actin networks in terms of filament length, mesh size and degree of bundling. Finally, we propose a model of network connectivity by investigating the effect of filament length on the mechanical properties and structure.

© 2009 Acta Materialia Inc. Published by Elsevier Ltd. All rights reserved.

1. Introduction

Cells sense, generate and respond to forces in their environment through cytoskeletal dynamics, and mechanical force plays important roles in fundamental cellular processes such as migration, cytokinesis and apoptosis [1–3]. Actin, one of the principal constituents of the cytoskeleton, contributes to the mechanical integrity of the cell and is involved in numerous cellular functions, organizing various microstructures according to functional demands [4,5]. Structural assembly of F-actin, critical in these processes, is regulated by over 100 actin-binding proteins (ABPs) [6,7]. Two major structures of F-actin organized by ABPs are the cross-linked network and the bundled filament. For example, the ABP filamin assembles filaments into three-dimensional orthogonal networks serving as a scaffold for cell motility and signaling [8,9]; in contrast, α -actinin at high concentration forms thick bundles contributing to structural stability of the cell, providing added mechanical strength [10,11]. Therefore, an understanding of cytoskeletal

mechanical properties governed by dynamic interactions between actin and ABPs is essential for understanding cell mechanics and the associated biological phenomena.

Cell experiments have revealed that the cytoskeleton exhibits both elastic and viscous characteristics under applied stress [12,13]. Since it is difficult to accurately characterize the mechanical properties of the cytoskeleton *in vivo* due to active remodeling as well as the presence of numerous other, uncontrolled factors, *in vitro* experiments on reconstituted gels of F-actin have proven useful [14–19]. *In vitro* studies have characterized the viscoelastic properties of F-actin polymerized from purified actin in combination with various ABPs. Many of these measurements of mechanical properties have been performed using a bulk rheometer, which yields global properties of the F-actin matrix. Discrepancies have been observed, however, between these large length scale measurements and microrheometry using micron-scale beads [20]. These have been attributed to a variety of factors, including the non-uniform local stress field, different deformation modes [21], the formation of a depletion zone around the microbead [22,23] and other effects present when the bead is comparable in size to the characteristic dimensions of the actin mesh and individual actin filaments, both of which tend to be on the scale of one to several microns [24]. While this similarity of length scales complicates

* Corresponding author. Address: Massachusetts Institute of Technology, Department of Mechanical Engineering, 77 Massachusetts Avenue, Room NE47-321, Cambridge, MA 02139, USA. Tel.: +1 617 253 5330; fax: +1 617 258 8559.

E-mail address: rdkamm@mit.edu (R.D. Kamm).

interpretation of the results of microrheometry, it also provides an opportunity to probe the local mechanical response and provide insight into the specific roles of ABP in mediating rheological behavior. Other *in vitro* experiments have demonstrated that actin gels stiffen with increasing strain up to a point, then rapidly soften as strain is further increased [15,25–29]. Actin networks under shear deformation exhibit an irreversible non-linear behavior, suggesting network remodeling and rupture of network bonds [26]. However, compressive force imposed on a dendritic actin network results in reversible stress softening, suggesting that it might be caused by a different mechanism such as filament buckling [27]. The mechanisms for both the increase and sudden fall in modulus remain a subject of debate. Although models to explain these findings of actin cytoskeleton have been proposed [19,27,30], observation of the network's response at the microscale will undoubtedly help elucidate the origin of this non-linear behavior.

Here we employ both passive and active microrheology to measure mechanical properties at the microscale using optical tweezers. Optical tweezers-based microrheology provides the advantage of high-precision force control in the range of 0.1–100 pN, while simultaneously monitoring the motion of the bead with nanometer resolution [31]. Although this technique has been used to measure viscoelastic properties of fd viruses and micellar solutions [32,33], its application to study F-actin networks has been limited [34]. In our passive approach, we track the motion of a thermally fluctuating microbead to estimate the frequency-dependent complex shear modulus of the F-actin network over a frequency range of 10^{-1} to 10^4 Hz. For the active approach, we apply a sinusoidal driving force to an embedded microbead and monitor its response to obtain the viscoelastic properties of the network. In particular, microscale non-linear behavior of F-actin network is demonstrated by performing the active measurement at large deformation.

We investigate the effect of ABPs on the mechanical properties of F-actin networks using both passive and active techniques. To correlate mechanical properties with structural geometry, both material properties and microstructure of the cross-linked F-actin network are probed as a function of ABP concentration. Confocal microscopy and total internal reflection fluorescent (TIRF) microscopy are used to visualize the F-actin networks organized with filamin, α -actinin and gelsolin. Unique features of F-actin networks polymerized with each ABP are visualized and quantified in terms of mesh size and degree of bundling. Average length of actin filaments is varied using gelsolin to investigate how the length of individual filaments alters network formation and its mechanical properties. While previous rheological measurements on entan-

gled F-actin solutions have demonstrated that particle thermal motions are more constrained as the length of filament increases and as mesh size decreases [16,35], to our knowledge, no comparable measurements have been reported in cross-linked F-actin networks. Based on our measurements, we propose a model to explain how the length of individual actin filaments influences connectivity of the cross-linked network and its elasticity.

2. Materials and methods

2.1. Microspheres

Amino functionalized beads (2.73% solids, Polybead Amino Microspheres; Polysciences, Warrington, PA) 0.5 and 1 μm in radius, were coated with mPEG-NHS (5 kDa; Nektar, San Carlos, CA) to prevent protein absorption as described previously [36] with the following modifications. Stock beads (40 μl) were diluted with 200 μl of deionized water. This solution was spun down for 10 min at 14,000 rpm, supernatant removed and the bead pellet resuspended with 200 μl of methanol. Next, the bead solution was again centrifuged as described above, the supernatant removed and the bead pellet resuspended with 200 μl of 10 mg ml^{-1} PEG-NHS diluted in one part DMSO and four parts methanol. After gently mixing the bead solution for 2 h at room temperature, the beads were stored at 4 $^{\circ}\text{C}$ with continuous rotation to prevent aggregation by sedimentation. Beads were used within 6 months of preparation.

2.2. Reconstituted *in vitro* F-actin networks

Lyophilized actin monomers and α -actinin both from rabbit skeletal muscle were purchased from Cytoskeleton Inc. (Denver, CO). The activity and purity of actin were tested with sodium dodecyl sulfate–polyacrylamide gel electrophoresis (SDS–PAGE). Polymerized actin filaments were separated from the non-polymerized G-actin by centrifugation at 100,000g for 40 min [37] and both supernatant and pellets were loaded on a 9% (w/v) PAGE gel. Protein bands stained with Coomassie blue showed that most of G-actin was polymerized into F-actin (Fig. 1A). Protein activity was confirmed by examining the geometry of polymerized actin filaments in the micrographs (Fig. 1B and C). Recombinant filamin-A was purified from Sf9 cell lysates [38] and recombinant human gelsolin is produced in *Escherichia coli* [39].

Actin monomers were diluted in fresh G-buffer (5 mM Tris–HCl, 0.2 mM CaCl_2 , 0.5 mM DTT, 0.2 mM ATP, pH 8.0) and incubated on

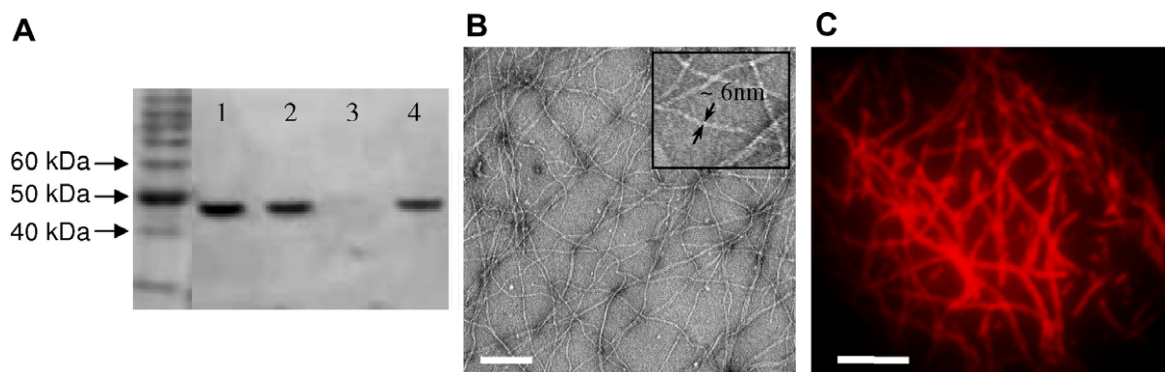


Fig. 1. Characterization of actin. (A) Scanned image of the polyacrylamide gel. Lane 1, G-actin kept overnight on ice; lane 2, G-actin after centrifuge without polymerization; lane 3, supernatant after centrifugation of polymerized actin; lane 4, pellet after centrifugation of polymerized actin. Bands observed in lanes 1 and 2 confirmed that actin is in monomeric form in G-buffer. In contrast to lane 4, no protein band is observed in lane 3, suggesting that most of the G-actin monomers are polymerized into F-actin during polymerization. (B) Electron microscope image of F-actin which are negatively stained with 2% uranyl acetate (scale bar, 200 nm). Inset: the diameter of actin filament is measured to be approximately 6 nm. (C) TIRF microscopy shows that the length of polymerized actin filaments are varying over 20 μm (scale bar = 5 μm).

ice for at least 2 h. Gelsolin, filamin or α -actinin were gently mixed with the actin monomer, followed by the addition of PEG-coated beads diluted in G-buffer. Actin polymerization was initiated by adding a tenth of the final volume of F-buffer (50 mM Tris–HCl, 500 mM KCl, 2 mM MgCl₂, 2 mM CaCl₂, 2 mM DTT, 5 mM ATP, 0.01% (w/v) NaN₃, pH 7.5). The sample was gently mixed by pipetting and immediately loaded into a custom-made flow chamber, with dimensions 25.8 mm × 8 mm × 0.1 mm (~20 μ l). Microspheres were firmly embedded in the F-actin network after several hours of polymerization. Concentrations of actin, filamin, α -actinin and gelsolin were varied depending on the experiment.

2.3. Characterizing F-actin microstructure

We visualized reconstituted F-actin structures polymerized with various ABPs and characterized them in terms of mesh size and degree of filament bundling. For visualization, fluorescently labeled actin (A-12373; Invitrogen, Carlsbad, CA) and rhodamine phalloidin (R415; Invitrogen, Carlsbad, CA) was used to stain actin filaments for confocal microscopy (Axiovert 200M; Carl Zeiss Inc., Thornwood, NY) and TIRF microscopy [40], respectively. For confocal microscopy, actin filaments were labeled by polymerizing regular actin monomers in the presence of labeled monomers at a molar ratio of 5:1. The sample was fixed by paraformaldehyde to minimize thermal fluctuations during image acquisition. A stack of 71 images was obtained with 100 nm separation to obtain the three-dimensional (3D) structure. Images were then deconvolved with HUYGENS ESSENTIAL software (Scientific Volume Imaging, Hilversum, The Netherlands) and assembled to construct the 3D image by IMARIS software (Bitplane, Zurich, Switzerland). We characterized the mesh size of the actin networks from two-dimensional (2D) plane images, instead of the projected images, in order to minimize the misinterpretation from a projection of 3D structure. The mesh size of the structure was determined by two methods. Each open area bounded by actin filaments was measured and the mesh diameter (ξ) was given by $\xi = (4 \times \text{Area}/\pi)^{1/2}$. Mesh size was also estimated by measuring the peak-to-peak distance in the intensity profiles of the images. Corrections to these 2D measurements for the three-dimensionality of the network were made according to Overby et al. [41].

2.4. Experimental setup using optical tweezers

Optical tweezers-based microrheology was performed using a custom-built instrument described previously [40]. Briefly, a high numerical aperture objective (100 \times , 1.40 NA, oil IR; Nikon, Tokyo, Japan) tightly focussed a 1064 nm laser (Coherent, Santa Clara, CA) at the specimen plane for optical trapping. The trap location was computer-controlled with a pair of orthogonally oriented acousto-optic deflectors (AODs) (Intra-Action, Bellwood, IL) and sample positioning was controlled using a piezo-stage (Polytech PI, Auburn, MA) with nanometer resolution. The combination of a 975 nm laser (Corning, Corning, NY) and a position sensitive device (PSD) (Pacific Silicon, West Lake Village, CA) was employed for back-focal plane position detection [42]. The 975 nm laser was operated at ~0.1 mW such that it formed a negligible trap with respect to the 1064 nm laser operated between 5 and 100 mW. The detection zone consisted of a circular area with radius of ~250 nm for 0.5 μ m radius beads and ~500 nm for 1.0 μ m beads. A second PSD was used to track the position of the trapping laser. The output voltages from both PSDs were collected by an A/D board (National Instruments, Austin, TX) and a custom program coded in LabView software (National Instruments, Texas, NI) was used to control experimental runs and data acquisition. Data analysis was performed using software written in MATLAB (Mathworks, Natick, MA).

Once the sample was loaded in the sample chamber and placed on the microscope stage, single beads were located and centered in the detection zone using an automated routine. After experimental runs (see below), the position of the bead was calibrated as described previously [43]. Optical tweezers were assumed to be a linear spring and the stiffness of the tweezers was characterized using free beads in buffer at different laser powers using standard calibration procedures [44].

2.5. Passive microrheology

Thermal fluctuations of an embedded bead, either 0.5 or 1.0 μ m in radius, were recorded at 50 kHz for ~42 s using the PSD. The complex compliance of the matrix, $\alpha(f)$, was computed from the power spectral density of the thermal motion using the fluctuation–dissipation theorem and the Kramers–Kronig relation [45]. The frequency-dependent complex shear modulus, $G(f)$, was determined by the generalized Stokes–Einstein relation, $G(f) = (6\pi a \alpha(f))^{-1}$, where a is the radius of the bead. The storage shear modulus, $G'(f)$, and loss shear modulus, $G''(f)$, were the real and imaginary components of $G(f)$, respectively. We also acquired G by capturing and analyzing the time-evolution of the mean square displacement, $\langle \Delta r^2(t) \rangle$ [46].

2.6. Active microrheology

Sinusoidal force was applied to a microsphere embedded in the F-actin matrix by oscillating the optical tweezers using AODs. The amplitude of the sinusoidal excitation by the optical tweezers was set to ± 200 nm and the frequency varied from 0.1 to 10 Hz. Positions of both the optical tweezers and microsphere were detected by two separate PSDs simultaneously. We fitted both the position of the trap, x_{trap} , and the position of the bead, x_{bead} , to sinusoidal functions of the form $A \sin(2\pi ft - \theta)$, where A is amplitude, t is time, f is frequency of the input sinusoidal function and θ is the phase of each signal. The force, $F(t)$, exerted on the matrix was computed using:

$$F(t) = k_{\text{trap}} [x_{\text{trap}}(t) - x_{\text{bead}}(t)], \quad (1)$$

where k_{trap} is the stiffness of the optical trap.

Since deformation of the matrix is given by x_{bead} , the frequency-dependent viscoelastic modulus was computed at a given frequency using:

$$G(f) = G'(f) + iG''(f) = \frac{\bar{F}(f)}{6\pi a \bar{x}_{\text{bead}}(f)} [\cos(\Delta\theta(f)) + i \sin(\Delta\theta(f))], \quad (2)$$

where \bar{F} is the force amplitude, $x_{\text{bead}}(t)$ is the amplitude of the bead response and $\Delta\theta$ is the phase delay between $F(t)$ and $x_{\text{bead}}(t)$.

To impose a large strain on the sample in the active measurement method, optical tweezers were used to trap an embedded microsphere of $a = 0.5$ μ m while moving the sample relative to the trap. The stage was moved sinusoidally with amplitudes of 400, 800 and 1600 nm at a frequency of 10 Hz. We monitored the response of the microsphere and fitted it to a sinusoidal function. Applied force was calculated from the distance of the microsphere from the center of the optical trap and k_{trap} . Network displacement was determined by calculating the difference between bead and stage displacements.

3. Results

3.1. Microstructures of F-actin networks

F-actin gels were prepared by polymerizing actin with filamin, α -actinin and gelsolin ([actin]/[gelsolin] = 250). They were visual-

ized by confocal microscopy as described in the Materials and methods section to investigate effects of cross-linking and bundling on F-actin network microstructure. For F-actin networks cross-linked with filamin, homogeneous networks were obtained over a range of the ratio of filamin to actin concentration (R_f) between 0.001 and 0.01 at a fixed actin concentration of 10 μM (Fig. 2A). When $R_f < 0.0001$, F-actin networks formed an inhomogeneous structure with large local variations, which is similar to the heterogeneity observed in F-actin networks cross-linked with low concentrations of heavy meromyosin [47]. When $R_f > 0.01$, the high concentration of filamin caused filament bundling and homogeneity of the network structure decreased consequently, as has also been reported in Goldmann et al. [48]. F-actin networks with $R_f = 0.01$ (Fig. 2A) exhibited nearly orthogonal branchings where actin filaments are cross-linked (Fig. 2B). For F-actin organized by α -actinin, as the relative concentration of α -actinin (R_α) to the fixed concentration of actin ($C_A = 10 \mu\text{M}$) increased, the degree of bundling increased as indicated by an increase in the relative fluorescent intensity of the filaments in confocal images (Fig. 2C). While a relatively homogeneous network was observed at low concentrations ($R_\alpha < 0.2$), actin filaments formed thick bundles at higher concentrations, making the F-actin/ α -actinin structure

inhomogeneous. In the magnified image (Fig. 2D) for $R_\alpha = 0.2$ (Fig. 2C), embedded bundles of actin filaments stand out compared to the smaller surrounding actin filaments. F-actin/filamin networks are characterized in terms of their mesh size, an important parameter in determining network mechanical properties. Mesh sizes for the homogeneous F-actin/filamin networks at both $R_f = 0.001$ and $R_f = 0.01$ were $\sim 1 \mu\text{m}$ (Fig. 3A and B), which is similar in value to the mesh size in a previous study of F-actin/scruin networks [49]. As expected, the mesh size of a cross-linked network was determined by the concentration of actin, and is relatively independent of the ABP concentration. In contrast, the mesh size of F-actin/ α -actinin networks increased with the concentration of α -actinin (Fig. 3C and D). As more filament bundles are formed with increasing R_α , bundling by α -actinin increases the mesh size of the F-actin network. The increase in degree of filament bundling is seen as an increase in normalized filament intensity (Fig. 3E).

3.2. Mechanical properties of F-actin networks

The mechanical properties of the F-actin networks were estimated by passive and active methods. For $C_A = 10 \mu\text{M}$ and

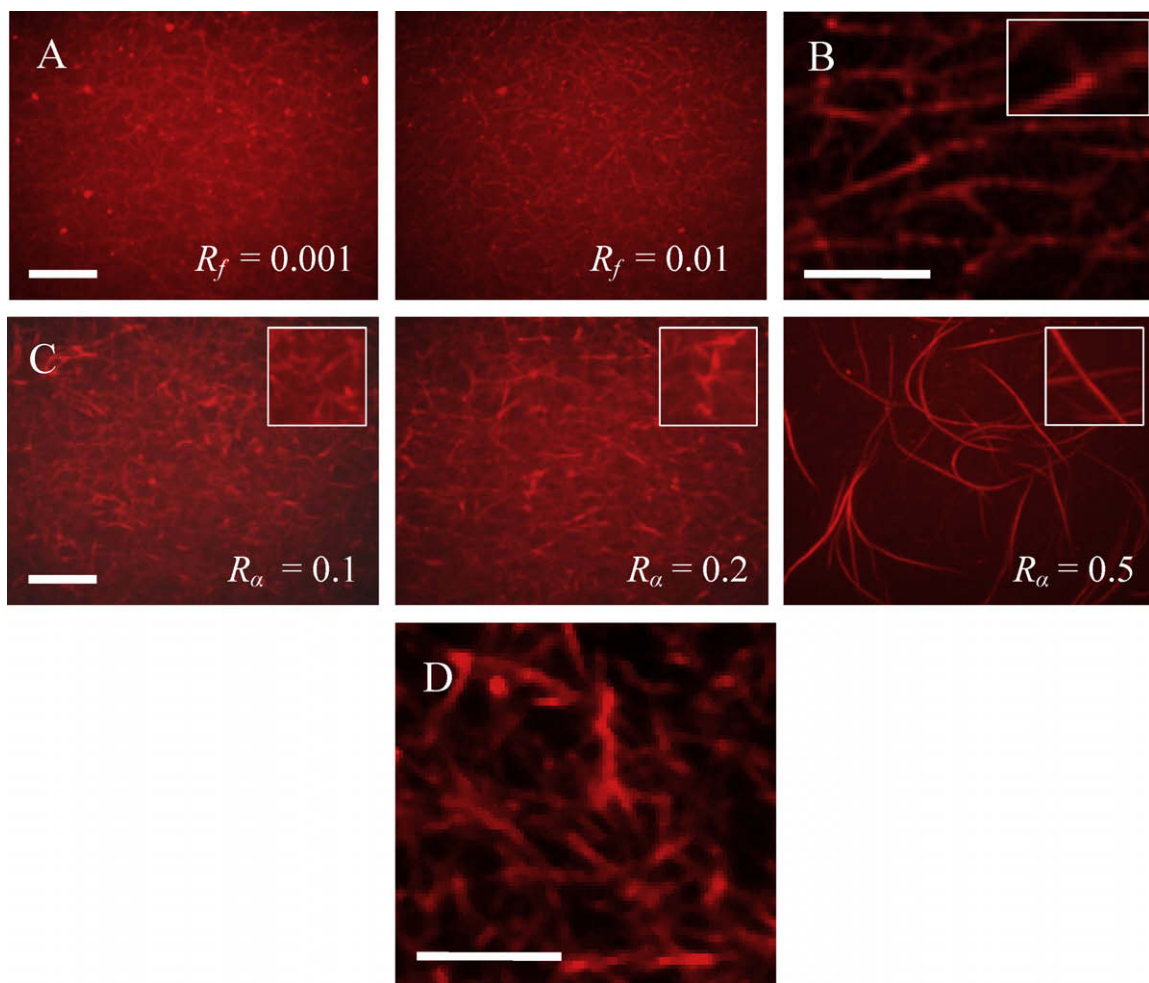


Fig. 2. Confocal microscopy of F-actin organized by actin-binding proteins. Images are projections of 71 layers each separated by 100 nm. (A) Confocal images of F-actin cross-linked with two different concentrations of filamin (scale bar = 10 μm). In a limited range of R_f between 0.001 and 0.01, the cross-linked F-actin networks exhibit uniform and fine microstructures. (B) Higher magnification of a single-layer image for F-actin cross-linked by filamin with $R_f = 0.01$ (scale bar = 5 μm). The image shows filamin forming F-actin cross-links at high angle. Inset: Magnification of the orthogonal cross-linking point. (C) Confocal images of F-actin organized with various concentrations of α -actinin (scale bar = 10 μm). Degree of bundling increases as the concentration of α -actinin increases relative to the concentration of actin. Inset: magnification of the actin filament bundles. (D) Higher magnification image of filaments with $R_\alpha = 0.02$ showing the evolution toward more highly bundled filaments (scale bar = 5 μm).

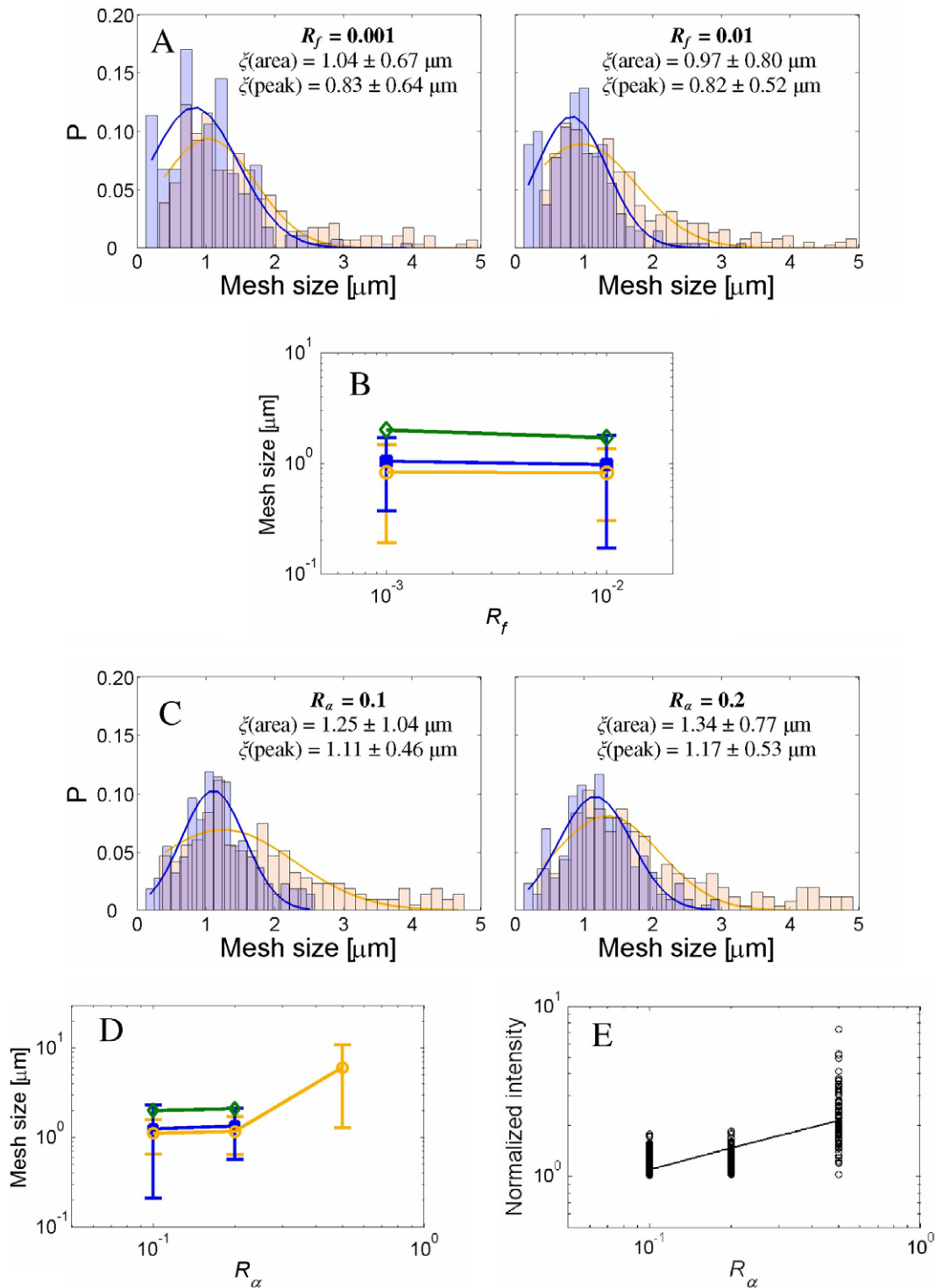


Fig. 3. Microstructural characterizations. Mesh sizes computed from the mesh area (orange) and the peak-to-peak distance (blue) in the images. 3D mesh size (green) is estimated using the properties of 2D meshes. (A) Distributions of mesh size, ζ , in the F-actin networks cross-linked with filamin at various R_f . (B) Mean and standard deviation of mesh size plotted against R_f . (C) Distributions of mesh size, ζ , in the F-actin networks organized by α -actinin at various R_α . (D) Mean and standard deviation of the mesh size plotted against R_α . As R_α increases, more filament bundles are formed and the mesh size of the networks increases. (E) Distributions of normalized intensity of the filaments in the F-actin networks at various R_α .

$R_f = 0.01$, the frequency-dependent shear modulus was estimated by passive measurement using the compliance function (Fig. 4A). At low frequency, G' dominated over G'' and approached a constant value. At high frequency, $G'' > G'$ and G' scaled as $f^{0.75}$ (Fig. 4A). Active measurements were performed at low amplitude, ± 200 nm, for the same F-actin/filamin network. The mechanical responses of the

microsphere to sinusoidal excitation have different phase delays and amplitudes depending on excitation frequency (see Fig. 4B). As frequency increases, viscous dissipation increased as indicated by the large hysteresis in the curves (Fig. 4B). Values for shear modulus of the F-actin network, calculated at each frequency (Fig. 4C) using Eq. (2), are in good agreement with the result

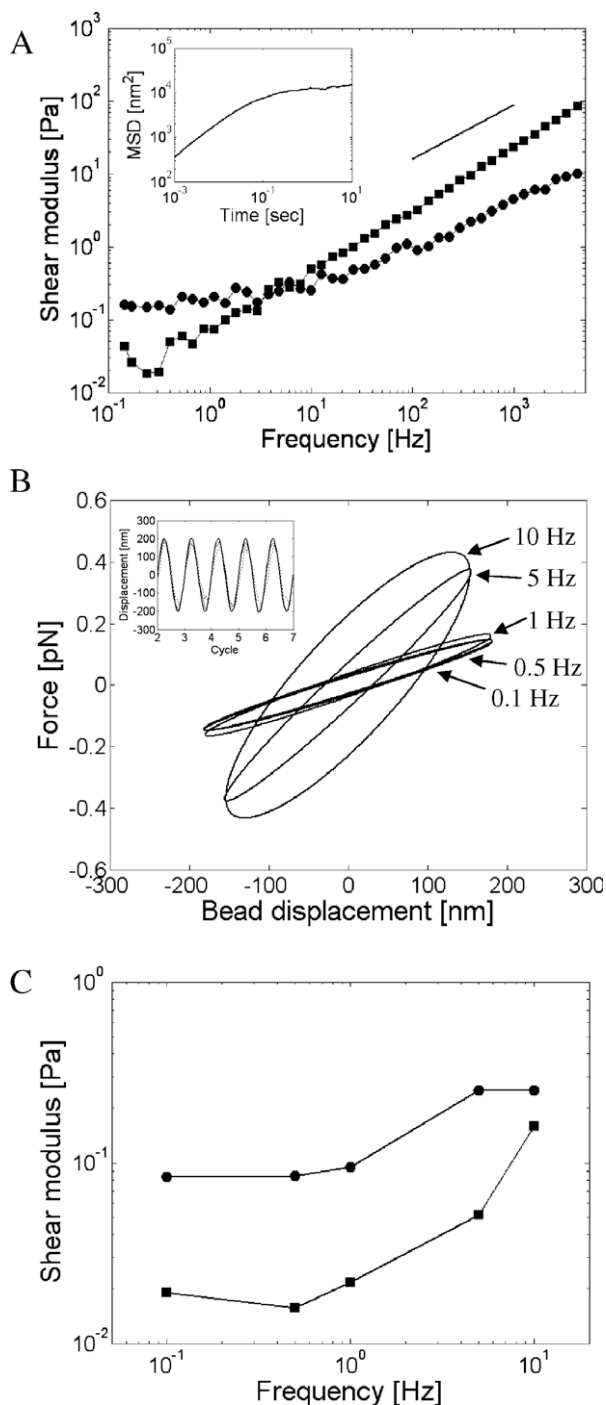


Fig. 4. Frequency-dependent mechanical properties in passive and active micro-rheology for F-actin networks with $C_A = 10 \mu\text{M}$ at $R_f = 0.01$. (A) Passive measurements; the complex shear moduli G' (circles) and G'' (squares) of F-actin networks are estimated over four decades of frequency by tracking the thermal fluctuations of an embedded microsphere. Solid line has a slope of 0.75. Inset: MSD of the microsphere. (B) Active measurements; a sinusoidal forcing applied to an embedded microsphere using optical tweezers. As the frequency increases, viscous dissipation increases as seen by a wider hysteresis in the force vs. bead displacement plot. Inset: sample traces of the position of the trapping laser (thick solid line) and the responses of a microsphere for 0.5 Hz (thin solid line) and 5 Hz (dotted line) excitation frequencies. (C) Storage (circle) and loss (square) moduli of F-actin network obtained using the active approach.

obtained by passive measurement in Fig. 4A. To investigate the effects of large strain, active measurements were performed over a range of amplitudes. As the displacements increase, the response

becomes non-linear as indicated by distortion of the force response (Fig. 5A) and the Lissajous curves (Fig. 5B). However, this micro-scale non-linear behavior is weak compared to the significant increase of modulus by strain-hardening observed in the bulk measurements [15,19]. In all other measurements of the mechanical properties, we set the excitation amplitude at a low level ($\pm 200 \text{ nm}$) to avoid non-linear effects.

The effect on mechanical properties of cross-linking with filamin was studied both actively and passively at $C_A = 10 \mu\text{M}$. As filamin concentration was increased from $R_f = 0.01$ to 0.04, both G' and G'' increased over the entire frequency range (Fig. 6A). Elastic effects became more dominant; relaxation frequency of the network (f_r), defined as the frequency when $G'(f_r) = G''(f_r)$, increased 23-fold as R_f increased four times. The complex shear moduli obtained by active and passive measurements are similar (Fig. 6B). The plateau storage shear modulus, G_0 , estimated as that at the minimum value in G'' over the range of frequencies tested, also increased 14-fold as R_f increased.

3.3. Effect of filament length on network elasticity and structure

We next investigated the effect of mean filament length on mechanical properties and microstructure of the cross-linked F-actin networks polymerized at $C_A = 10 \mu\text{M}$, $R_f = 0.01$ and in the presence and absence of gelsolin to regulate filament length. In the addition of gelsolin, the molar ratio of gelsolin to actin was 1:1000. To quantify the effect of gelsolin on filament length, we visualized single actin filaments polymerized in the presence and absence of gelsolin. While some long filaments are observed in the TIRF image for the actin polymerized in the absence of gelsolin (Fig. 7A), the addition of gelsolin decreased the lengths of the filaments significantly (Fig. 7B). Measurements from such micrographs showed the average filament length to be 8.2 ± 5.2 and $2.2 \pm 1.4 \mu\text{m}$ for the actin filaments polymerized in the absence and presence of gelsolin, respectively (Fig. 7C and D). Cross-linked F-actin networks organized by actin filaments with different average lengths were also visualized. TIRF images show that actin filaments in networks polymerized without gelsolin (Fig. 8A) are much longer than those in networks polymerized with gelsolin (Fig. 8B). In the confocal images too, long filaments are observed only in the network without gelsolin (Fig. 8C). Mesh sizes in the network appear to be independent of gelsolin, and therefore, independent of the length of the actin filaments forming the network (Fig. 8E and F). However, both G' and G'' measured passively decrease as the length of actin filaments decreases (Fig. 8G). Plateau values seen in the MSD curves (inset in Fig. 8G) suggest that greater steric and elastic constraints are imposed in networks polymerized with longer actin filaments. The relaxation times $= f_r^{-1}$ are approximately 0.2 s for both short- and long-filament networks. Mechanical properties measured by the active method exhibit similar behavior, having comparable values of both G_0 and f_r (Fig. 8H).

Networks were also probed using microspheres with $a = 1 \mu\text{m}$. With the large microspheres as well, both G' and G'' measured by the active method agree well with corresponding values obtained with passive rheology. Agreement between the two methods does not depend on the average length of filaments as compared in Fig. 9A (no gelsolin) and B (with gelsolin). Relaxation times for both networks are similar, $\sim 1 \text{ s}$, but larger than the 0.2 s relaxation time found in measurements with the smaller microsphere, $a = 0.5 \mu\text{m}$. G_0 decreases as the average length of actin filament decreases (Fig. 9C). Although there is a discrepancy in G_0 between measurements made with $a = 0.5 \mu\text{m}$ and $a = 1 \mu\text{m}$, G_0 of the network without gelsolin is higher than that with gelsolin, indicating that, when the network is formed by

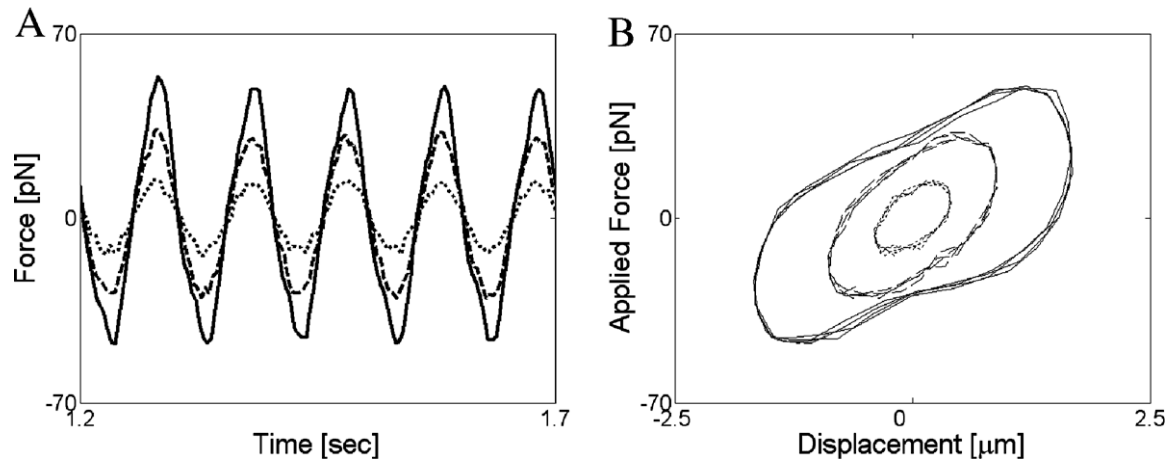


Fig. 5. Mechanical behavior of cross-linked F-actin network subject to large oscillatory deformation. Symbols in the figures correspond to the applied deformation: 400 nm (...), 800 nm (- - -) and 1600 nm (-). (A) Force vs. time. The amplitude of force increases as the applied deformation increases. As indicated by the distortions in the force curves, the network exhibits a non-linear response at large deformation. (B) Corresponding Lissajous figure. The ellipsoidal Lissajous curve is deformed by the non-linear behavior at large deformation.

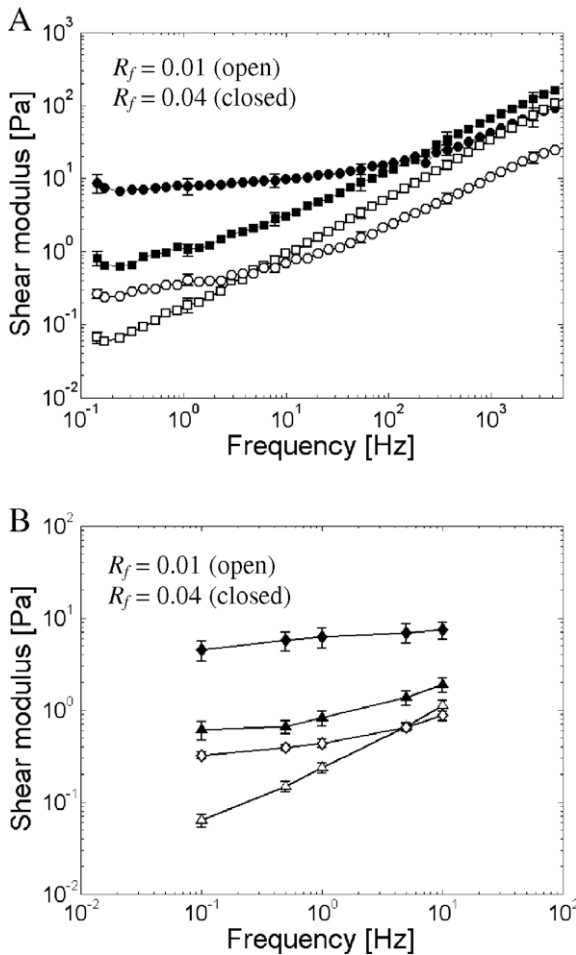


Fig. 6. Effect of cross-linker fractional concentration, R_f , on complex shear modulus. Storage and loss shear moduli are estimated for $C_A = 10 \mu\text{M}$ at $R_f = 0.01$ (open) and $R_f = 0.04$ (closed). G' (circle) and G'' (square) by passive method, G' (diamond) and G'' (triangle) by active method. In both passive (A) and active (B) measurements, shear moduli increase as R_f increases.

long filaments, fluctuations of the embedded microsphere are more confined.

4. Discussion

In these experiments, we investigated the effects of actin filament length, method of measurement (active vs. passive and small vs. large probe), degree of cross-linking, and strain amplitude on the frequency-dependent shear moduli of reconstituted actin gels using a carefully characterized system. Other studies have typically reported the effects of these parameters individually, and few have studied the effect of filament length and strain-dependent rheology at the microscale. In addition, because minor differences in experimental protocol can lead to significant effects on measured moduli, we felt that it would be useful to have one complete set of measurements examining these multiple effects in a single system under tight control.

Passive and active microrheology produce similar results for F-actin networks, provided the strains are small and in the linear regime. We employed two complementary methods to measure gel microrheology. In the passive approach, the frequency-dependent complex modulus was obtained over four decades in frequency by tracking thermal fluctuations of microspheres embedded in F-actin networks. The F-actin networks exhibit a plateau modulus (G_0) and a low G'' indicative of solid-like behavior at low frequencies. However, at high frequencies, G' exhibits a significantly greater frequency-dependence compared to the weak power law observed in cells [13,50]. In active measurements, the complex shear modulus is estimated by monitoring the mechanical response to the external force imposed by optical tweezers. Previous studies showed that actin and myosin networks exhibit different viscoelastic responses when measured by the active method compared to the passive method, which was attributed to tension in the filaments induced by myosin [34]. Since our system lacks motor proteins and applied strains are small and in the linear response range, the active and passive results show good agreement for our cross-linked F-actin networks. To a varying degree depending on measurement methods, the mechanical moduli (G' and G'') of the *in vitro* F-actin networks tend to be smaller than those obtained from some measurements of living cells [12,13,51]. This difference has been attributed to the internal stresses in living cells arising from actomyosin contraction, external adhesion and potentially to the complexity of the cytoskeletal structure with the wide variety of ABPs found in a cell [34,51]. It is also important to note that our approaches are limited in that they probe local mechanical

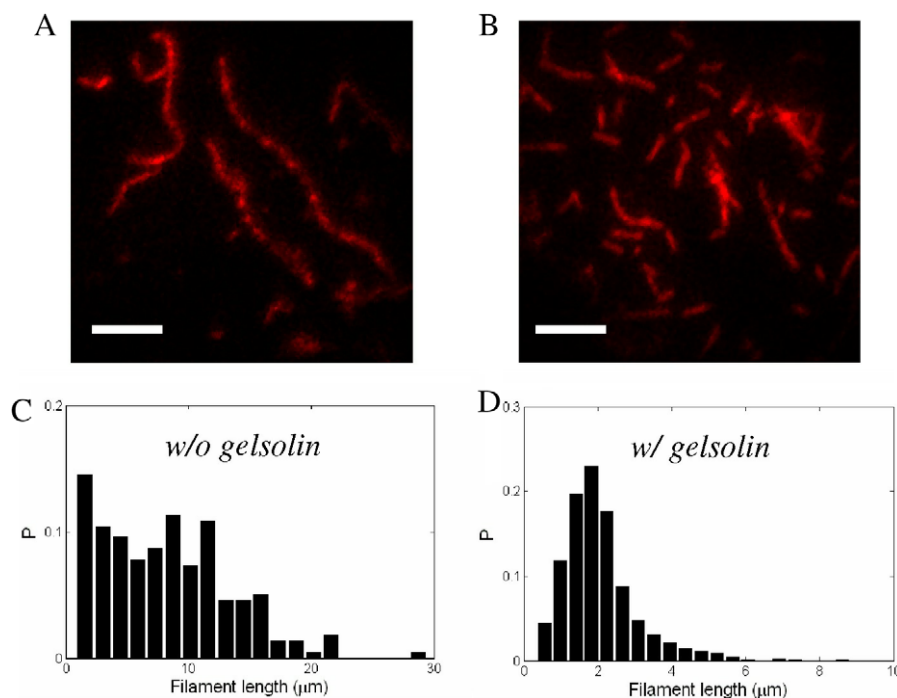


Fig. 7. Effect of gelsolin on filament length. Micrographs show that actin filaments polymerized in the absence of gelsolin (A) are much longer than those in the presence of gelsolin (B). Length distributions for both conditions are obtained by measuring the length of single actin filaments from micrographs (C and D).

properties by monitoring the motion of a single particle. Single-particle microrheology can be sensitive to the local environment of the embedded particle and the degree to which the particle is coupled to the matrix. Two-point microrheology overcomes these limitations by measuring the correlated motion of two particles [52]. As the length scale in the correlated motion is much larger than the size of the particle, two-point microrheology better reflects the bulk mechanical properties.

Employing the active measurement method, we were able to observe the microscale non-linear behavior of a cross-linked F-actin network. When loading amplitude is increased, in the present experiment by increasing the amplitude of stage oscillation, the force response of an F-actin network becomes non-linear, resulting in a distortion of the Lissajous figures (Fig. 5B). This strain-dependent non-linear behavior at the microscale is qualitatively analogous to the mechanical properties of reconstituted actin gels under pre-stress probed at the macroscale [15,26,27] in that G' is observed to increase as the bead amplitude increases. However, the non-linearity observed in the present measurements is considerably smaller. The difference can be attributed to several factors. It should be noted that the strain and stress estimated here are not the differential values which have been measured in the macroscopic measurement with pre-stress using a rheometer [15], but rather, the total amounts in response to progressively larger sinusoidal oscillations of the bead. Also, in the macroscopic measurements, applied shear stress produces a non-affine deformation of the cross-linked F-actin network [53,54], inducing extension in some actin filaments and compression in others. As the thermal undulation in the stretched filaments is reduced, network elastic modulus increases. By contrast, in our microscale measurements, local excitation using a probe particle deforms only nearby filaments within a characteristic distance comparable to the size of the probe particle. While the macroscale method estimates global properties by measuring the response of the entire network, active microrheology probes local, microscale mechanical properties at force levels in the physiological range. Therefore, our techniques

can be applied to probe the characteristics of individual cross-links as studied in single molecule assays [55]. Further study of strain-dependent microrheology for F-actin networks cross-linked with other ABPs will provide a better understanding of the microscopic origin of non-linear behavior in the F-actin networks.

The effects of ABP concentration are similar at the microscale to previous macroscale measurements. As filamin concentration increases for a given concentration of actin, G_0 increases 14 times as R increases four times. This is approximately consistent with previous macroscale studies showing a scaling of $G_0 \sim R^\beta$, with typical exponent, β from 0.4 to 2 depending on the ABP used [17,18,49]. For example, a short and rigid ABP, scruin, has a scaling exponent of 2 and heavy meromyosin (HMM) follows the scaling $G_0 \sim R^{1.2}$. As the dependence of G_0 on R reflects the molecular characteristics of the ABP (e.g., molecular structure, binding affinity and degree of dimerization [18]), filamin would appear to behave in a manner more similar to scruin than to HMM. It should be noted, however, that scaling of the modulus as a function of ABP varies depending on the magnitude of R [26,47]. For the pre-stressed and highly cross-linked actin networks, the moduli are remarkably insensitive to concentrations of actin and ABP [15].

The elasticity of the F-actin network is influenced by the length of actin filaments constituting the network. Gelsolin, a severing and capping protein, was used to regulate the contour length of actin filaments [56] and mechanical properties of the network polymerized in the absence and presence of gelsolin were compared (Fig. 8). *In vitro*, F-actin polymerizes to contour lengths, L , of about 2–70 μm with a mean length of 20 μm [57] and the average length of actin filaments can be adjusted by the concentration of gelsolin [56]. The gelsolin concentration used in these experiments regulates L to be 2 μm , consistent with Janmey et al. [56]. The G_0 of cross-linked F-actin networks formed in the absence of gelsolin is higher than that in the presence of gelsolin, similar to the behavior seen with entangled F-actin solutions [16,20]. However, the effect on G_0 of gelsolin is smaller for cross-linked F-actin networks than for entangled F-actin solutions. While the elastic response

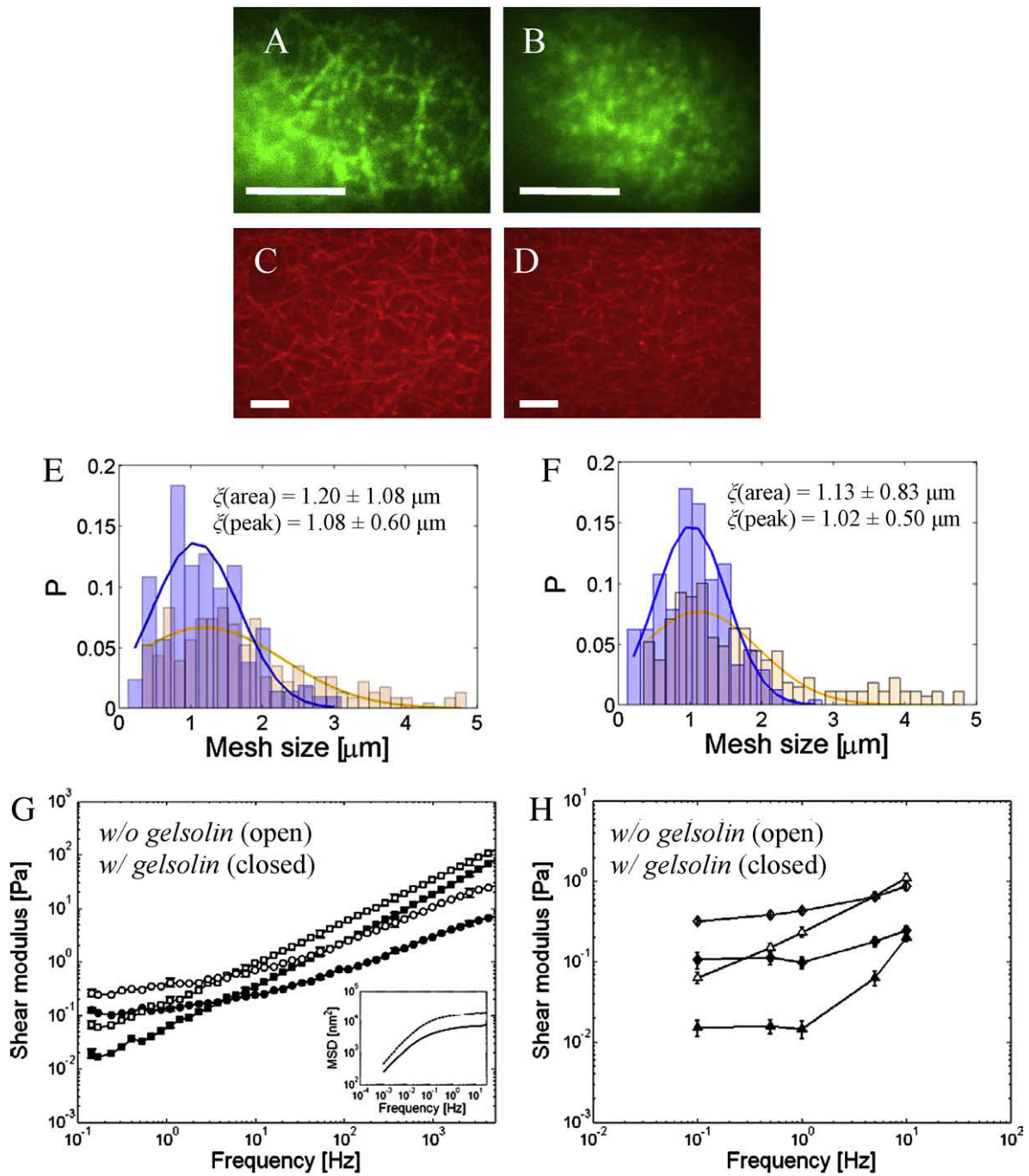


Fig. 8. Effect of gelsolin on microstructure and microrheology of F-actin network. TIRF (A and B) and confocal microscopy (C and D) images of F-actin/filamin network polymerized in the absence (A and C) and presence (B and D) of gelsolin (scale bar = 10 μm). Although longer actin filaments are observed in the F-actin network polymerized in the absence of gelsolin, the mesh size distributions obtained by two different methods (see text for details) are similar for the network without gelsolin (E) and the network with gelsolin (F). Frequency-dependent shear moduli of F-actin networks without gelsolin (open symbols) and with gelsolin (closed symbols) are measured using passive (G) and active (H) methods. G' (circle) and G'' (square) by passive method, G' (diamond) and G'' (triangle) by active method. The moduli obtained from the two methods exhibit similar results. Both G' and G'' are higher for the F-actin network polymerized in the absence of gelsolin (longer filaments) over the entire frequency range. Inset in (G): MSD curves for the F-actin networks in the presence (dotted) and absence (solid) of gelsolin.

of F-actin solutions is dominated by the entanglement length, L_e , the elasticity of an F-actin network is determined by the distance between cross-link points, L_c . Assuming affine deformations, the plateau storage shear modulus G_0 of a cross-linked F-actin network can be described by [58]:

$$G_0 \sim \frac{\kappa^2}{kT} \xi^{-2} L_c^{-3}, \quad (3)$$

where ξ is the mesh size, κ is the bending modulus of actin filament, k is Boltzmann's constant, and T is the absolute temperature. If the networks with filamin are mostly cross-linked with negligible bundling, κ and ξ should not change with filament length as confirmed by our confocal images (Fig. 2) and their characterizations (Fig. 3). L_c in Eq. (3) is determined by the concentration of cross-linking protein [17]. We note, however, that Eq. (3) does not account for the effects of filament length. When the actin filament length is much

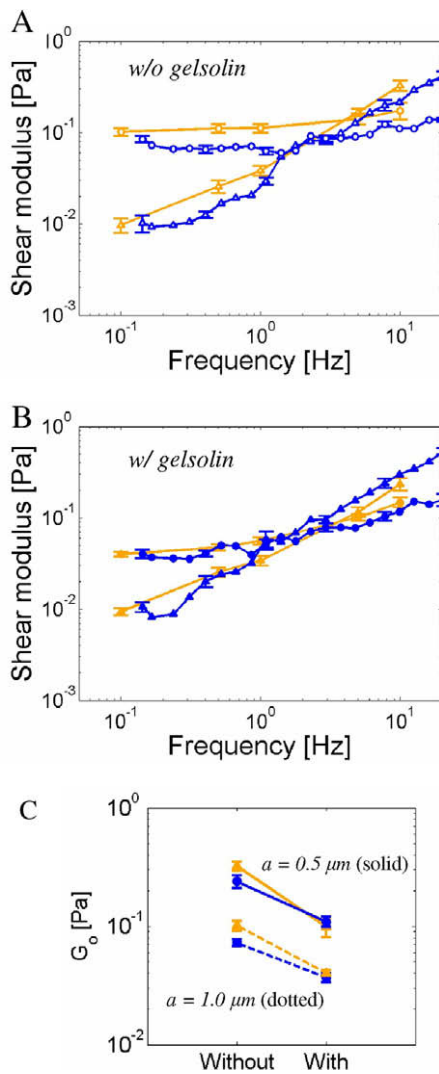


Fig. 9. Effects of probe size, filament length and measurement method on microrheology of cross-linked F-actin networks. Using a larger microsphere with radius $a = 1 \mu\text{m}$, the complex shear moduli are estimated for the F-actin networks polymerized in the absence (A) and presence (B) of gelsolin. G' (circle) and G'' (triangle) by passive (blue) and active (orange) methods. Both passive and active measurements exhibit similar results independent of filament length. (C) Comparison of G_0 obtained by passive (blue circles) and active (orange triangles) measurements for the F-actin network with and without gelsolin. F-actin networks formed with short filaments are less stiff than those formed with long filaments. The decrements in G_0 are similar, independent of the microsphere's dimension (solid: $a = 0.5 \mu\text{m}$; dotted: $a = 1 \mu\text{m}$).

larger than the mesh size, most ABPs cross-link filaments at the intersection points, forming a well-defined, highly interconnected network. In contrast, if the length of actin filaments is comparable to, or only slightly greater than, the mesh size, many loose ends exist, which contribute little to the overall stiffness of the network. (Imagine the filaments of Fig. 10A being cut at random locations.) Reducing the length of individual filaments leads to more loose ends in the network configuration, thereby altering network connectivity. The resulting effect is a network that is less capable of withstanding stress, and therefore exhibits a smaller modulus. Our findings therefore suggest that the mechanical response of cross-linked actin networks to external force is affected by filament length, which affects network connectivity, as well as L_c . Network connectivity can be investigated by visualizing cross-linking proteins as well as actin filaments. We tried to obtain the images of cross-linkers in a 3D actin network using filamin conjugated with fluorescent dye. However, it was difficult to identify individual cross-linking proteins because of the high background signal and thermal fluctuations of actin network that prevented us from obtaining clear images.

The size of the probe particle also has an effect on measured network viscoelasticity. To further investigate the effects of characteristic length scales in F-actin network microrheology, mechanical properties of F-actin network were probed using a larger microsphere ($a = 1 \mu\text{m}$) and the results compared to those obtained with the smaller one ($a = 0.5 \mu\text{m}$). The G_0 of the network with $L = 20 \mu\text{m}$ is consistently higher than that with $L = 2 \mu\text{m}$; however, values of G_0 are approximately 2- to 3-fold lower when measured using the larger microsphere as compared to the smaller one (Fig. 9C). That is, the elastic modulus of the F-actin network probed by the tracer whose diameter is comparable to the length of actin filaments (and mesh size) is smaller than that measured by the probe tracer which is much smaller than the filament length. Interestingly, a significant transition in G_0 has been observed in entangled F-actin solutions when the average length of actin filaments is close to the diameter of the microsphere used in the measurements [16,20], which could, in both cases, be attributable to a local depletion zone created in the vicinity of a probe tracer. In network formation, long actin filaments are depleted from the immediate vicinity of the microsphere through a combination of their high bending stiffness and steric exclusion. Therefore, the microsphere resides in an environment that is more viscous than elastic, leading to a reduced G' but having little impact on G'' . This is reflected in the observation that the larger microsphere exhibits a smaller relaxation frequency (f_r) at which $G' = G''$. Also the larger microsphere exhibits a scaling $G'' \sim f^{0.85}$ at high frequency indicating that the local environment behaves in a manner more reminiscent of a

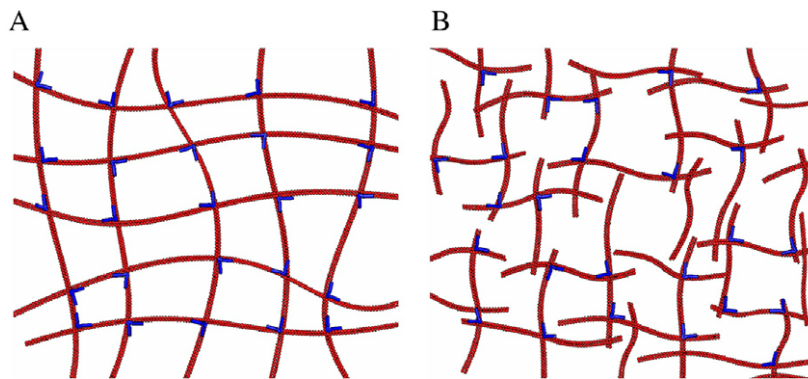


Fig. 10. Schematic illustrations of F-actin network organized by long (A) and short (B) actin filaments at identical concentrations of actin filaments and cross-linkers. In the network with long filaments (A), most filaments are attached at each crossing point by ABPs that are arranged regularly along the filaments. In contrast, the network with short filaments (B) forms incomplete loops with many loose ends, and their arrangement is random compared to the network in (A). This difference in structure would cause the network with short filaments to be less stiff than the one with long filaments.

Newtonian fluid as compared to the scaling $G'' \sim f^{0.75}$ observed with $a = 0.5$ and $L = 20 \mu\text{m}$.

5. Conclusions

We employed methods of passive and active microrheology using optical tweezers and observed the mechanical properties of homogeneous F-actin networks. The microscale non-linear behavior of the cross-linked F-actin network was obtained by active measurement at high strain. The effects of length scale on both network elasticity and microstructure were investigated by controlling actin filament length and probe size. We showed that short actin filaments influence connectivity of the network structure resulting in a reduced elasticity. The results presented here, and future similar studies with different actin-binding proteins, will provide insight into the microscopic origin of mechanical properties in cross-linked F-actin networks.

Acknowledgements

We are grateful to T.P. Stossel for helpful discussions. This work was supported by the NIGMS (GM076689) (to H.L. and R.D.K.), an NSF Career Award (0643745) (to M.J.L.), an Nicholas Hobson Wheelers, Jr. Fellowship (to J.M.F.), the W.M. Keck Foundation (to M.J.L.), the Westaway Research Fund (to M.J.L.), and the Singapore-MIT Alliance for Research and Technology.

Appendix A. Figures with essential colour discrimination

Certain figures in this article, particularly Figures 1–3 and 7–10, are difficult to interpret in black and white. The full colour images can be found in the on-line version, at doi: [10.1016/j.actbio.2009.10.044](https://doi.org/10.1016/j.actbio.2009.10.044).

References

- Janmey PA, McCulloch CA. Cell mechanics: integrating cell responses to mechanical stimuli. *Annu Rev Biomed Eng* 2007;9:1–34.
- Khan S, Sheetz MP. Force effects on biochemical kinetics. *Annu Rev Biochem* 1997;66:785–805.
- Vogel V, Sheetz M. Local force and geometry sensing regulate cell functions. *Nat Rev Mol Cell Biol* 2006;7:265–75.
- Bartles JR. Parallel actin bundles and their multiple actin-bundling proteins. *Curr Opin Cell Biol* 2000;12:72–8.
- Stossel TP, Fenteany G, Hartwig JH. Cell surface actin remodeling. *J Cell Sci* 2006;119:3261–4.
- dos Remedios CG, Chhabra D, Kekic M, Dedova IV, Tsubakihara M, Berry DA, et al. Actin binding proteins: regulation of cytoskeletal microfilaments. *Physiol Rev* 2003;83:433–73.
- Pollard TD, Cooper JA. Actin and actin-binding proteins. A critical evaluation of mechanisms and functions. *Annu Rev Biochem* 1986;55:987–1035.
- Stossel TP, Condeelis J, Cooley L, Hartwig JH, Noegel A, Schleicher M, et al. Filamins as integrators of cell mechanics and signalling. *Nat Rev Mol Cell Biol* 2001;2:138–45.
- Feng Y, Walsh CA. The many faces of filamin: a versatile molecular scaffold for cell motility and signalling. *Nat Cell Biol* 2004;6:1034–8.
- Meyer RK, Aebi U. Bundling of actin filaments by alpha-actinin depends on its molecular length. *J Cell Biol* 1990;110:2013–24.
- Wachsstock DH, Schwartz WH, Pollard TD. Affinity of alpha-actinin for actin determines the structure and mechanical properties of actin filament gels. *Biophys J* 1993;65:205–14.
- Bausch AR, Moller W, Sackmann E. Measurement of local viscoelasticity and forces in living cells by magnetic tweezers. *Biophys J* 1999;76:573–9.
- Fabry B, Maksym GN, Butler JP, Glogauer M, Navajas D, Fredberg JJ. Scaling the microrheology of living cells. *Phys Rev Lett* 2001;87:148102.
- Claessens MMAE, Tharmann R, Kroy K, Bausch AR. Microstructure and viscoelasticity of confined semiflexible polymer networks. *Nat Phys* 2006;2:186–9.
- Gardel ML, Nakamura F, Hartwig JH, Crocker JC, Stossel TP, Weitz DA. Prestressed F-actin networks cross-linked by hinged filamins replicate mechanical properties of cells. *Proc Natl Acad Sci USA* 2006;103:1762–7.
- Liu J et al. Microrheology probes length scale dependent rheology. *Phys Rev Lett* 2006;96:118104.
- Tharmann R, Claessens MMAE, Bausch AR. Viscoelasticity of isotropically cross-linked actin networks. *Phys Rev Lett* 2007;98:088103.
- Wagner B, Tharmann R, Haase I, Fischer M, Bausch AR. Cytoskeletal polymer networks: the molecular structure of cross-linkers determines macroscopic properties. *Proc Natl Acad Sci USA* 2006;103:13974–8.
- Xu JY, Tseng Y, Wirtz D. Strain hardening of actin filament networks—regulation by the dynamic cross-linking protein alpha-actinin. *J Biol Chem* 2000;275:35886–92.
- Schmidt FG, Hinner B, Sackmann E. Microrheometry underestimates the values of the viscoelastic moduli in measurements on F-actin solutions compared to macrorheometry. *Phys Rev E* 2000;61:5646–53.
- Maggs AC. Micro-bead mechanics with actin filaments. *Phys Rev E* 1998;57:2091–4.
- Levine AJ, Lubensky TC. Two-point microrheology and the electrostatic analogy. *Phys Rev E* 2002;65:011501.
- Morse DC. Viscoelasticity of concentrated isotropic solutions of semiflexible polymers. 2. Linear response. *Macromolecules* 1998;31:7044–67.
- Schmidt CF, Barmann M, Isenberg G, Sackmann E. Chain dynamics, mesh size, and diffusive transport in networks of polymerized actin—a quasielastic light-scattering and microfluorescence study. *Macromolecules* 1989;22:3638–49.
- Gardel ML, Nakamura F, Hartwig J, Crocker JC, Stossel TP, Weitz DA. Stress-dependent elasticity of composite actin networks as a model for cell behavior. *Phys Rev Lett* 2006;96:088102.
- Gardel ML, Shin JH, MacKintosh FC, Mahadevan L, Matsudaira P, Weitz DA. Elastic behavior of cross-linked and bundled actin networks. *Science* 2004;304:1301–5.
- Chaudhuri O, Parekh SH, Fletcher DA. Reversible stress softening of actin networks. *Nature* 2007;445:295–8.
- Storm C, Pastore JJ, MacKintosh FC, Lubensky TC, Janmey PA. Nonlinear elasticity in biological gels. *Nature* 2005;435:191–4.
- Janmey PA, Hvidt S, Lamb J, Stossel TP. Resemblance of actin-binding protein actin gels to covalently cross-linked networks. *Nature* 1990;345:89–92.
- Janmey PA, McCormick ME, Rammensee S, Leight JL, Georges PC, MacKintosh FC. Negative normal stress in semiflexible biopolymer gels. *Nat Mater* 2007;6:48–51.
- Brau RR et al. Passive and active microrheology with optical tweezers. *J Opt A Pure Appl Opt* 2007;9:S103–12.
- Addas KM, Schmidt CF, Tang JX. Microrheology of solutions of semiflexible biopolymer filaments using laser tweezers interferometry. *Phys Rev E* 2004;70:021503.
- Atakhorrami M, Schmidt CF. High-bandwidth one- and two-particle microrheology in solutions of wormlike micelles. *Rheol Acta* 2006;45:449–56.
- Mizuno D, Tardin C, Schmidt CF, MacKintosh FC. Nonequilibrium mechanics of active cytoskeletal networks. *Science* 2007;315:370–3.
- Wong IY, Gardel ML, Reichman DR, Weeks ER, Valentine MT, Bausch AR, et al. Anomalous diffusion probes microstructure dynamics of entangled F-actin networks. *Phys Rev Lett* 2004;92:178101.
- Valentine MT, Perlman ZE, Gardel ML, Shin JH, Matsudaira P, Mitchison TJ, et al. Colloid surface chemistry critically affects multiple particle tracking measurements of biomaterials. *Biophys J* 2004;86:4004–14.
- Zuchero JB. In vitro actin assembly assays and purification from *Acanthamoeba*. *Methods Mol Biol* 2007;370:213–26.
- Nakamura F, Osborn E, Janmey PA, Stossel TP. Comparison of filamin A-induced cross-linking and Arp2/3 complex-mediated branching on the mechanics of actin filaments. *J Biol Chem* 2002;277:9148–54.
- Kwiatkowski DJ, Janmey PA, Yin HL. Identification of critical functional and regulatory domains in gelsolin. *J Cell Biol* 1989;108:1717–26.
- Brau RR, Tarsia PB, Ferrer JM, Lee P, Lang MJ. Interlaced optical force-fluorescence measurements for single molecule biophysics. *Biophys J* 2006;91:1069–77.
- Overby D, Ruberti J, Gong HY, Freddo TF, Johnson M. Specific hydraulic conductivity of corneal stroma as seen by quick-freeze/deep-etch. *J Biomech Eng Trans ASME* 2001;123:154–61.
- Gittes F, Schmidt CF. Back-focal-plane detection of force and motion in optical traps. *Biophys J* 1998;74:A183.
- Lang MJ, Asbury CL, Shaevitz JW, Block SM. An automated two-dimensional optical force clamp for single molecule studies. *Biophys J* 2002;83:491–501.
- Neuman KC, Block SM. Optical trapping. *Rev Sci Instrum* 2004;75:2787–809.
- Chaikin PM, Lubensky TC. Principles of condensed matter physics. Cambridge: Cambridge University Press; 1995.
- Mason TG, Weitz DA. Optical measurements of frequency-dependent linear viscoelastic moduli of complex fluids. *Phys Rev Lett* 1995;74:1250–3.
- Luan Y, Lileeg O, Wagner B, Bausch AR. Micro- and macro-rheological properties of isotropically cross-linked actin networks. *Biophys J* 2008;94:688–93.
- Goldmann WH, Tempel M, Sprenger I, Isenberg G, Ezzell RM. Viscoelasticity of actin-gelsolin networks in the presence of filamin. *Eur J Biochem* 1997;246:373–9.
- Shin JH, Gardel ML, Mahadevan L, Matsudaira P, Weitz DA. Relating microstructure to rheology of a bundled and cross-linked F-actin network in vitro. *Proc Natl Acad Sci USA* 2004;101:9636–41.
- Hoffman BD, Massiera G, Van Citters KM, Crocker JC. The consensus mechanics of cultured mammalian cells. *Proc Natl Acad Sci USA* 2006;103:10259–64.
- Wang N, Tolic-Norrelykke IM, Chen J, Mijailovich SM, Butler JP, Fredberg JJ, et al. Cell prestress. I. Stiffness and prestress are closely associated in adherent contractile cells. *Am J Physiol Cell Physiol* 2002;282:C606–16.
- Crocker JC, Valentine MT, Weeks ER, Gislser T, Kaplan PD, Yodh AG, et al. Two-point microrheology of inhomogeneous soft materials. *Phys Rev Lett* 2000;85:888–91.

- [53] Head DA, Levine AJ, MacKintosh EC. Deformation of cross-linked semiflexible polymer networks. *Phys Rev Lett* 2003;91:108102.
- [54] Onck PR, Koeman T, van Dillen T, van der Giessen E. Alternative explanation of stiffening in cross-linked semiflexible networks. *Phys Rev Lett* 2005;95:178102.
- [55] Ferrer JM, Lee H, Chen J, Pelz B, Nakamura F, Kamm RD, et al. Measuring molecular rupture forces between single actin filaments and actin-binding proteins. *Proc Natl Acad Sci USA* 2008;105:9221–6.
- [56] Janmey PA, Peetermans J, Zaner KS, Stossel TP, Tanaka T. Structure and mobility of actin-filaments as measured by quasi-elastic light-scattering, viscometry, and electron-microscopy. *J Biol Chem* 1986;261:8357–62.
- [57] Kaufmann S, Kas J, Goldmann WH, Sackmann E, Isenberg G. Talin anchors and nucleates actin filaments at lipid membranes. A direct demonstration. *FEBS Lett* 1992;314:203–5.
- [58] Mackintosh FC, Kas J, Janmey PA. Elasticity of semiflexible biopolymer networks. *Phys Rev Lett* 1995;75:4425–8.